Departement für klinische Diagnostik und Services, Klinik für Bildgebende Diagnostik
der Vetsuisse-Fakultät Universität Zürich

Vorsteherin Departement: Prof. Dr. med. vet. Regina Hofmann-Lehmann
Direktor Klinik: Prof. Dr. med. vet., PhD, Dipl. ECVDI Patrick R. Kircher

Arbeit unter wissenschaftlicher Betreuung von
Dr. med. vet., PhD, Dipl. ECVDI Francesca Del Chicca

Change of the hepatic apparent diffusion coefficient and hepatic fat fraction in healthy cats during body weight gain

Inaugural-Dissertation

zur Erlangung der Doktorwürde der
Vetsuisse-Fakultät Universität Zürich

vorgelegt von

Gian-Luca Marcus Steger

Tierarzt
von Chur, Graubünden

genehmigt auf Antrag von

Prof. Dr. med. vet., PhD, Dipl. ECVDI Patrick R. Kircher, Referent

2020

Inhaltsverzeichnis

Summary

Objective: To describe the change in the mean hepatic apparent diffusion coefficient (ADC) and hepatic fat fraction (HFF) during body weight (BW) gain in cats using MRI.
Animals: Twelve healthy adult male cats.
Procedures: The cats underwent MRI examination. Sequences included multiple echo GRE MRI, and diffusion-weighted MRI (DW-MRI) (b-values: 0, 400, 800 s/mm^2) at time point 0. After 40 weeks of being fed with high energy food ad libitum, the cats underwent a second MRI examination (time point 1). In different regions of interest (ROIs) in the liver parenchyma, BW, HFF, and the ADC were recorded at the two time points.
Results: At time point 0 and 1, respectively, the median BW was 4.5 kg (range, 3.6–5.3 kg) and 6.5 kg (range, 4.3–8.7 kg); the mean HFF was 3.39 ± 0.89% and 5.37 ± 1.92%; the mean hepatic ADC was 1.21 ± 0.08 × 10–3 mm^2/s and 1.01 ± 0.2 × 10–3 mm^2/s. Statistically significant differences between the two time points were found for BW, HFF, and the ADC. The HFF was positively associated with the BW, the ADC was negatively associated with HFF.
Conclusions and clinical relevance: The hepatic ADC depends on factors related to the patient. Similar to humans, cats exhibit decreased hepatic ADC with increased HFF. Protons associated with fat tissue may reduce diffusivity, resulting in a lower ADC than in liver with lower HFF. Additional studies in cats with different nutritional states and over longer periods are necessary to further investigate these findings.

Zusammenfassung

Zielsetzung: Beschreibung der Veränderung des mittleren scheinbaren Diffusionskoeffizienten (ADC) und der Leberfettfraktion (HFF) bei Katzen während der Gewichtszunahme mittels MRT.
Tiere: Zwölf gesunde männliche erwachsene Katzen.
Durchführung: Zwei MRI Untersuchungen, mit multiple echo GRE MRI und diffusion-weighted MRI (DW-MRI) Sequenzen, wurden durchgeführt. 40 Wochen nach Fütterung einer hochenergetischen Nahrung ad libitum erfolgte die zweite Untersuchung.
Das Körpergewicht (KG) sowie die HFF und der ADC in verschiedenen ROIs des Leberparenchyms wurden gemessen.
Resultate: Der Median des KG der ersten Messung lag bei 4.5 kg (3.6 – 5.3 kg) und der zweiten bei 6.5 kg (4.3 – 8.7 kg). Der Mittelwert der HFF lag bei der ersten Messung bei 3.39 ± 0.89% und bei der zweiten bei 5.37 ± 1.92%. Der Mittelwert des ADC lag bei der ersten Messung bei $1.21 \pm 0.08 \times 10{-}3$ mm^2/s, bei der zweiten bei $1.01 \pm 0.2 \times 10{-}3$ mm^2/s. Statistisch signifikante Unterschiede zwischen den zwei Zeitpunkten wurden für das KG, die HFF und den ADC gefunden. Die HFF ist positiv assoziiert mit dem KG und der ADC negativ mit der HFF.
Zusammenfassung und klinische Relevanz: Der ADC hängt von patientenbezogenen Faktoren ab. Wie beim Menschen gezeigt werden konnte, führt eine Erhöhung der HFF zu einer Senkung des hepatischen ADC. Mit Fettgewebe assoziierte Protonen könnten die Diffusionsfähigkeit verringern, was bei hoher HFF zu einem niedrigeren ADC führt als bei Lebergewebe mit niedriger HFF.

Change of the hepatic apparent diffusion coefficient and hepatic fat fraction in healthy cats during body weight gain

Gian-Luca Steger, DVM; Elena Salesov, Dr med vet; Henning Richter, Dr med vet, PhD; Claudia E. Reusch, Dr med vet; Patrick R. Kircher, Dr med vet, PhD; Francesca Del Chicca, Dr med vet, PhD

Clinic for Diagnostic Imaging (Steger, Richter, Kircher, Del Chicca) and Clinic of Small Animal Internal Medicine (Salesov, Reusch), Vetsuisse Faculty, University of Zurich, Winterthurerstrasse 258c, 8057 Zurich, Switzerland.

Acknowledgments

The authors declare that there were no conflicts of interest. The authors thank Prof. Torgerson for the assistance with the statistical analysis.

Address correspondence to Dr. Francesca Del Chicca at fdelchicca@vetclinics.uzh.ch

Abstract

Objective: To describe the change in the mean hepatic apparent diffusion coefficient (ADC) and hepatic fat fraction (HFF) during body weight (BW) gain in cats using MRI.

Animals: Twelve healthy adult male cats.

Procedures: The cats underwent MRI examination. Sequences included multiple echo GRE MRI, and diffusion-weighted MRI (DW-MRI) (b-values: 0, 400, 800 s/mm^2) at time point 0. After 40 weeks of being fed with high energy food ad libitum, the cats underwent a second MRI examination (time point 1). In different regions of interest (ROIs) in the liver parenchyma, BW, HFF, and the ADC were recorded at the two time points.

Results: At time point 0 and 1, respectively, the median BW was 4.5 kg (range, 3.6–5.3 kg) and 6.5 kg (range, 4.3–8.7 kg); the mean HFF was 3.39 ± 0.89% and 5.37 ± 1.92%; the mean hepatic ADC was 1.21 ± 0.08 × 10^{-3} mm^2/s and 1.01 ± 0.2 × 10^{-3} mm^2/s. Statistically significant differences between the two time points were found for BW, HFF, and the ADC. The HFF was positively associated with the BW, the ADC was negatively associated with HFF.

Conclusions and clinical relevance: The hepatic ADC depends on factors related to the patient. Similar to humans, cats exhibit decreased hepatic ADC with increased HFF. Protons associated with fat tissue may reduce diffusivity, resulting in a lower ADC than in liver with lower HFF. Additional studies in cats with different nutritional states and over longer periods are necessary to further investigate these findings.

Abbreviations

ADC	Apparent diffusion coefficient
BW	Body weight
DW-MRI	Diffusion-weighted MRI
FHL	Feline hepatic lipidosis
HFF	Hepatic fat fraction
GRE	Gradient recalled echo
PDFF	Proton density fat fraction
ROI	Region of interest
T0	Initial time point zero
T1	Time point one

Introduction

DW-MRI is a functional imaging method that allows a qualitative and quantitative assessment of liver tissue diffusivity. Historically, the use of DW-MRI has been described for brain investigations[1-4], but an emerging application of DW-MRI in veterinary medicine is the examination of abdominal organs.

In human medicine, DWI-MRI is used in routine MRI examination of the liver and enables the detection of focal lesions and diffuse hepatic diseases.[5] The ADC is derived from DWI-MRI images and represents the quantification of the random motion of water molecules in biological tissues. It has been shown to be an adequate method for predicting liver fibrosis and inflammation and is used to help differentiate between benign and malignant focal lesions.[6] The ADC is, though, dependent on patients characteristics, among others, the HFF.

The association of reduced ADC with higher HFF has been reported in humans, as well as in a murine model.[5,7-9] Other studies could not find a correlation between HFF and the ADC.[10]

Hepatic fat accumulation with consequent increased HFF occurs in domestic cats secondary to obesity, [11] and pathological conditions as diabetes, [12] and FHL.[13] Overweight and obesity are increasing problems in cats, [14] and FHL is the most common hepatobiliary disorder in adult cats. [13,15] Obesity and FHL are also correlated processes: obese cats have a significant higher liver fat concentration than lean cats, [16] so those that are overweight and obese are at risk for the development of FHL. Increased HFF is clinically difficult to quantify, and its clinical significance may be variable. Noninvasive techniques to evaluate hepatic fat content in clinical practice are usually limited to ultrasound and computer tomography, but both modalities lack specificity and allow only semiquantitative evaluation of fat content.[17] Assessment of hepatic steatosis for clinical care requires not only diagnosis but also grading of severity.

In human medicine, hepatic steatosis is a pathogenic, potentially reversible condition and there is an urgent need, in both clinical and research arenas to detect its presence and to assess its severity.[18] The same needs are shared by veterinary medicine.

A substantial number of studies, mostly in humans, demonstrated that MRI allows a noninvasive, accurate, reproduceable, precise, and reader-independent quantification of HFF regardless of the degree of hepatic lipidosis.[19,20,17,21-26] One recently commercially released multiple echo GRE pulse sequence enables accurate and consistent measurement of HFF.[27]

To the authors' knowledge, no study has investigated the correlation of the hepatic ADC and HFF in cats. The purpose of the present study was to investigate the effect of increasing HFF on the ADC of the feline liver during BW gain in healthy cats. This effect could affect the interpretation of DW-MRI on hepatic parenchyma.

Materials and Methods

The present prospective sample survey study was approved by the Cantonal Veterinary Office of Zurich (license number, ZH118-16) in accordance with the Animal Welfare Act of Switzerland and as a part of a main concurrent study.

The cats underwent two MRI examinations at the initial time point (T0) and 40 weeks later at time point 1 (T1).

Animals

Twelve neutered male adult research purpose-bred shorthair cats were enrolled in this study. At T0, all cats underwent a clinical examination. Based on a physical examination, hematological and biochemical tests, all cats were deemed to be in good health, except two cats with mild elevated renal values (chronic kidney disease stage 2 according to International Renal Interest Society guidelines). Ten cats were classified as American Society of Anesthesiologists I; the two cats with elevated renal values were classified as American Society of Anesthesiologists II.

At T1, the physical examination, hematological and biochemical tests were repeated in all cats. Ten cats were confirmed classified as American Society of Anesthesiologists I; the two cats classified as American Society of Anesthesiologists II were excluded from the second examination due to causes that are not related to the study.

The BW of the cats was recorded before each MRI examination. After the initial MRI examination, the cats were fed a commercial dry food[a] ad libitum for 16 weeks or until they were overweight (body condition score, 7/9). Subsequently, the amount of food was adjusted to maintain this BW.

Anesthesia

The cats were fasted for 12 h before anesthesia. Premedication consisted of ketamine (10 mg/kg), midazolam (0.1 mg/kg), and butorphanol (0.3 mg/kg) intramuscularly. After

premedication, a catheter was aseptically placed in the left or right cephalic vein for administration of contrast medium, IV medication, and lactated Ringer's solution (3 mL/kg/h).

Oxygen was administered via a facemask for 30 min prior to anesthesia induction. Anesthesia was induced with alfaxalone (0.5–2 mg/kg) intravenously. After induction, the cats were intubated with a cuffed endotracheal tube and mechanically ventilated with positive end-expiratory pressure in a pressure-controlled mode (5–11 cm H_2O). The respiratory rate was adjusted to achieve an end-tidal CO_2 of 35–42 mmHg (4.66–5.59 kPa).

The anesthesia was maintained using isoflurane with a 1:1 ratio of oxygen and air. Anesthesia was monitored and recorded with a multiparameter monitor that included spirometry, capnography, and an MRI-compatible wireless respiratory sensor, as well as vectorcardiography and pulse oximetry.

Glycopyrrolate (10 mcg/kg, IV) was administered if the pulse rate fell below 100 bpm for longer than 10 min. If necessary, this procedure was repeated once.

MRI

All cats were placed in dorsal recumbency in a 3 Telsa MRI scanner[b] with a phased-array anterior coil.[c] MRI examination included morphological images to exclude liver abnormalities. Performed sequences were as follows: T2-weighted (turbo spin echo; repetition time/echo time, 2,000/80 ms; flip angle, 90°; field of view, adapted to animal; voxel size, 1.18/1.42/3.00 mm; slice thickness, 3 mm; slice gap, 0 mm) and T1-weighted precontrast sequence (mDixon, gradient echo; repetition time/echo time 1/echo time 2, 3.7/1.21/2.4 ms; flip angle, 10°; field of view, adapted to animal; voxel size, 1.5/1.5/3.00 mm; slice thickness, 3 mm; slice gap, -1.5 mm).

For the fat quantification, a multiple echo GRE (multi-echo acquisition, multi-peak mDIXON sequence with T2* correction)[d] was performed. The following sequence parameters

were used: breath hold, expiration; repetition time/echo time 1/delta echo time, 7.5/1.23/1.0 ms; flip angle, 3°; field of view, adapted to animal; slice thickness, 4 mm; slice gap, -2 mm; acquired voxel size, 1.5/1.49/4 mm; echoes, 6. The breath hold technique was used for a maximum of 21.3 s. Therefore, controlled mechanical ventilation was discontinued to force brief expiratory apnea and was continued immediately after the sequence.

DWI-MRI was performed (3b imaging performance sensitivity encoding) with the following parameters: repetition time/echo time, 1.8 s/75 ms; flip angle, 90°; field of view, adapted to animal; slice thickness, 4 mm; slice gap, 0.4 mm; acquired voxel size, 1.96/1.83/4 mm; number of b-values, 3 (0, 400, 800 s/mm^2).

The following T1-weighted postcontrast sequence was performed after hand injection of contrast medium[e] (0.3 mL/kg, IV), followed by a 10 mL saline (0.9% NaCl) solution: mDixon, gradient echo; repetition time/echo time 1/echo time 2, 3.7/1.21/2.4 ms; flip angle, 10°; field of view, adapted to animal; voxel size, 1.5/1.5/3.00 mm; slice thickness, 3 mm; slice gap, -1.5 mm).

All images were acquired in the transverse plane.

Postprocessing and data analysis

Postprocessing of the multiple echo GRE sequence was performed on the workstation of the previously described MRI unit, and DW-MRI was performed on a dedicated extended workstation.[f]

HFF was evaluated qualitatively and quantitatively. The qualitative evaluation was performed using a color-coded map. Tissue with no fat content is displayed in dark violet. Progressively increasing fat component is displayed as gradually brighter colors (from violet to blue, green, yellow, and orange). Fat component of approximately 80% to pure fat tissue is displayed in red. For the quantitative evaluation of HFF, 4 ROIs of similar size were manually drawn on the liver parenchyma using an adjustable round cursor on the automatically

generated fat fraction images. The ROIs were drawn in the right cranial, right caudal, middle, and left liver parenchyma. Based on the DW-MRI, the software automatically generated a ADC map. Three ROIs of similar size were manually drawn on the liver parenchyma using an adjustable round cursor on the ADC map. The ROIs were drawn in the middle right, middle left, and cranial liver parenchyma in areas with subjectively homogeneous signal intensity as otherwise described.[28] In all cases, care was taken to avoiding major blood vessels, the gallbladder, and obvious image artifacts.

Statistical analysis

Statistical analyses were performed using a free software environment for statistical computing.[g] Descriptive statistics were calculated, and numerical data were reported as the mean ± SD, median and range, or numbers (%) where appropriate.

Normal distribution was tested using the Shapiro-Wilk test, and significant differences in paired data were determined using the Wilcoxon test. The relationship between the ADC and HFF was analyzed using a generalized mixed effect model. The relationship between the BW and HFF was also analyzed using a generalized mixed effect model.

P-values were considered to be significant when less than 0.05.

Results

Twelve cats were evaluated at T0; at T1, 10 were evaluated. The median age at the beginning of the study was 77 months (range, 75–78 months). The physical examination, hematological and biochemical tests of hepatic panel were unremarkable in all cats at T0 and T1. At T0, median BW was 4.52 kg (range, 3.6–5.3 kg) and a T1 was 6.35 kg (range, 4.3–8.7 kg). This difference in BW was statistically significant between the two time points ($p < 0.001$).

The mean acquisition time was 99.76 ± 12.65 s for the T2-weighted sequence; 10.85 ± 2.75 s for T1-weighted precontrast; 9.27 ± 2.37 s for T1-weighted postcontrast; 3 min 28 s ± 47 s for diffusion-weighted imaging; and 14.3 ± 1.7 s for the multiple echo GRE sequence.

The morphological images of all feline livers were considered unremarkable in T2- and T1-weighted precontrast and postcontrast sequences at both time points. All livers were homogeneous hyperintense to the epaxial musculature and hypointense to the spleen on T2-weighted images, homogeneously and mildly hyperintense to epaxial muscles and spleen on precontrast T1-weighted images, and homogenously hyperintense to epaxial muscles and spleen and on postcontrast T1-weighted images.

Regarding the qualitative assessment of the livers using the color-coded map of the multiple echo GRE sequence at T0, the livers of 3 cats were almost completely dark violet with only traces of bright violet. The dark violet component was subjectively more extensive than the bright violet component in the other 9 cats. At T1, the livers of 3 cats exhibited dark and bright violet components with subjectively equal distribution. In the other 7 cats, the bright violet component was subjectively more extensive than the dark violet component. No cases showed visible blue areas (Figure 1).

The mean HFF was 3.39 ± 0.89% at T0 and 5.37 ± 1.92% at T1, with a statistically significant difference between the two time points ($p = 0.005$) (Figure 2). The mean hepatic ADC was 1.21 ± 0.08 × 10^{-3} mm^2/s at T0 and 1.01 ± 0.2 × 10^{-3} mm^2/s at T1, with a statistically significant difference between the two time points ($p = 0.037$) (Figure 3). The changes and the relationship between BW, HFF, and ADC at T0 and T1 is shown in Figure 4.

The mean ROI size for HFF measurements was 95.6 ± 3.1 mm^2 (96.6 ± 3.4 mm^2 at T0 and 94.6 ± 3.8 mm^2. at T1), with no statistically significant difference between the two time points ($p = 0.114$). The median size of the ROI on the ADC map was 51.4 ± 9.2 mm^2 (50.1 ± 12.0 mm^2

at T0 and 52.8 ± 4.9 mm^2 at T1), with no statistically significant difference between the two time points ($p = 0.314$).

The generalized mixed effect models suggested that the hepatic ADC was negatively associated with BW ($p < 0.001$), as well as negatively associated with HFF measured using the multiple echo GRE sequence ($p < 0.001$). The model predicts a 0.29% reduction in the ADC for every 1% increase in HFF, when the other variables related to the cats were kept constant.

Discussion

Our study showed that one of the factors influencing the hepatic ADC in cats is HFF. An increase in HFF measured with the multiple echo GRE sequence following BW gain is associated with significantly reduced ADC. As conditions related to increased HFF in cats are common, this association must be considered when DW-MRI of the liver is performed to avoid misinterpretation. MRI is increasingly used in veterinary medicine to assess liver disease due to its potential diagnostic value. So far, DW-MRI of the feline liver has only been reported in a small group of healthy cats.[28]

In human medicine, studies have shown that determining the ADC is a useful imaging method to help differentiate benign and malignant liver lesions to predict the severity of hepatic fibrosis and monitor the progress of treatment response.[6,29-32] The ADC is a common index derived from DW-MRI sequences and quantifies the diffusion of water molecules within biological tissue.[33] The sensitivity of the imaging sequence to water diffusion can be altered by determine the b-value. In the present study, the b-values of 0, 400, and 800 s/mm^2 were chosen to obtain images with an acceptable spatial resolution, and considering the current literature. Three b-values were used to deliver a more accurate calculation of the ADC.[33,34]

However, in a clinical setting, comparing the hepatic ADC between patients should be exercised with caution because the value depends on many technical factors and factors related to the patient. Technical factors that can influence the ADC are field strength, imaging platform, applied gradients strength and magnitude (b-values), coils, different manufactures, software, acquisition parameters, and other factors.[35-37] In the present study, these bias factors were minimized because the two examinations included the same equipment and sequence parameters. Factors related to the patient that can influence the ADC include patient age[38], motion from neighboring organs[39], and pathological processes such as hepatic steatosis.[40] Being the same cats evaluated twice, also variation of factors related to the patients have been minimized, and is reasonable to assume that the change in ADC truly depends on the HFF and BW gain, the only factors that significantly changed between the 2 time points.

Regarding technical considerations, we used in the present study, a free-breathing technique due to the shorter acquisition time and the impossibilities of a triggered sequence in cats, considering the shallow respiration movements. In addition, the free-breathing method is recommended in humans.[41]

DW-MRI sequences in abdominal studies are still not routinely used in veterinary medicine. Despite equipment requirements and high costs, this technique is promising as non invasive diagnostic tool in hepatic diseases. The technical advantages of DW-MRI include the following: brief scanning times due to new technologies (mean of 3 min 28 s), which makes its use in standard protocols for clinical examinations possible, and the avoidance of exogenous contrast agent. The major technical disadvantages of DW-MRI are the limited spatial resolution, sensitivity to artifacts, and need for general anesthesia. Literature on DW-MRI applied to liver examination is still lacking in feline medicine, with no studies documenting variability of ADC.

Liver biopsy is currently accepted as the gold standard for determining increased liver fat content and FHL[23]. Liver biopsy has important limitations: it is an invasive technique that can cause pain, transient hypotension, and other complications such as bleeding, infections, bile leakage, pneumothorax, and hemothorax.[42,43] Furthermore, it is not a suitable technique for follow up. Hepatic fat accumulation can be heterogeneously distributed across the liver, so a biopsy sample may not be representative of the pathological processes and lead to a non accurate estimation of hepatic fat.[43,44] Clinically, the severity of FHL is histologically assessed by estimating the percentage of hepatocytes containing fat droplets. Thus, interpretation of the biopsy is subjective and semiquantitative.[45]As a result, alternative methods for screening and monitoring increased HFF and FHL, and clinical decision-making are needed.[23,43,44,46]

The multiple echo GRE sequence allows PDFF measurements for the estimation of HFF due to a pixel-by-pixel reconstruction algorithm-based separation between water and fat and creates a water-only, fat-only, in-phase, opposed-phase, fat fraction and T2* images. In humans, PDFF measurements have been determined to be a reliable and reproducible estimation of HFF across different manufacturers and field strengths.[27] Sequences based on multiple echo GRE techniques with fat-water separation, yield quantification of the HFF highly correlated with the estimation of HFF validated mean other invasive and noninvasive techniques.[47,48 49,50]

This correlation has been described between values obtained by PDFF and HFF values obtained mean MRI-spectroscopy and histology (among others[51]). In particular, the correlation between HFF measured with PDFF techniques and other invasive or noninvasive techniques has been reported in dogs[24], geese[52], and mice.[53]

The primary advantages of the described multiple echo GRE sequence are that it allows visualization and then assessment of the entire liver parenchyma and that images are

produced in a single breath hold. The lack of ionizing radiation, the short time of investigation, and the repeatability of the results make the described multiple echo GRE sequence a suitable tool for monitoring disease and evaluating therapy efficacy. Beside the quantitative analysis of the HFF mean drawing of ROIs, a color-coded map can be created. That allows visually display of the amount of fat in the liver, and enables convenient comparison of images acquired at T0 and T1 in the same regions, or comparison between multiple echo GRE images and other sequences. In the analyzed cats, increased HFF was apparent even on images comparison only. The distribution of the different colors reflects the uniformity of fat accumulation in the present study. That could represent an important clinical application of the technique, mainly in cats with higher HFF than the population of the present study.

For a more precise quantification of the HFF, multiple ROIs have been drawn on the hepatic parenchyma. The choice of the number, location and size of the ROIs was based on the available literature on human medicine [54] and on healthy dogs.[24]

In human medicine, a negative correlation similar to our data between HFF and ADC has been found.[5,7,9] The current hypothesis is that fat droplets inside hepatocytes and extracellular fat accumulation impedes the movement of water, resulting in a reduction in the ADC. [5] It is likely that, similarly to what is described in human medicine, also in the examined cats, protons associated with intra- and extracellular fat reduce the interstitial space and reduce diffusivity.

Inflammation and fibrosis may be additional causes for a reduction in the ADC, as other studies postulated in human medicine. [5] In the present study, concurrent diseases were considered unlikely, based on the normal morphological images and the lack of biochemical abnormalities in the hepatic panel at both time points.

The two primary limitations of the present study were its small sample size and limited observation period, both due to animal welfare reasons. The positive association between BW gain and HFF is expected. Our data show that the HFF increases, during BW gain, in a relatively short period of time. The maximum mean HFF in the cats of our study was 5.37%. In human medicine, hepatic lipidosis is defined by a PDFF greater than 5.6% assessed by quantitative fat-water separation MRI in adult patients [55] and greater than 5% in children.[56] No corresponding data are available in feline medicine, but taking these data as reference, the HFF of the analyzed cats are at the cut off values of the definition of FHL. These cats, though, were defined as healthy, so it is possible the increased HFF could indicate an early and pre-clinical stage of FHL.

Moreover, PDFF and hepatic triglyceride content was not biochemically confirmed from liver biopsies. A histological examination of the liver parenchyma would have not provided quantification of HFF but may have excluded concurrent diseases at the histological level.

Due to the different spatial resolutions of the DW-MRI and multiple echo GRE images, it was not possible to draw the ROIs exactly in the same localization of the hepatic parenchyma. Thus, some degree of spatial mismatch between the locations of the two measurements must be taken into account. In this study, the increase in HFF was limited and achieved in a relatively short period of time. Further studies conducted over a longer period in cats with a higher body condition score and higher HFF, as well in animals with FHL, are needed to completely understand the correlation between the ADC, HFF and BW. We would expect an even more marked correlation between the ADC and HFF during longer observation periods.

Our study suggests that the hepatic ADC is negatively associated with the HFF following BW gain, and this association should be considered when interpreting DW-MRI of the liver.

Footnotes

a. Hill's™ Science Diet™ Adult Optimal Care, Hill's Pet Nutrition.

b. Philips Ingenia 3.0T scanner, Philips AG Healthcare, 8027 Zurich, Switzerland.

c. dStream Torso, coil solution, 32 channels, Philips AG Healthcare, 8027 Zurich, Switzerland.

d. mDIXON Quant, Philips AG Healthcare, 8027 Zurich, Switzerland.

e. Omniscan® (Gadodiamid), GE Healthcare AG, 8152 Glattbrugg, Switzerland.

f. Philips Intellispace Portal 2.6.3.5, Philips Medical System, Best, Netherlands.

g. R (version 3.2.3) and RStudio software (version 1.1.456, RStudio, Boston, USA) for Mac OS.

References

1. Moseley ME, Cohen Y, Mintorovitch J, et al. Early detection of regional cerebral ischemia in cats: comparison of diffusion- and T2-weighted MRI and spectroscopy. *Magn Reson Med* 1990;14:330-346.

2. Mizoguchi S, Hasegawa D, Hamamoto Y, et al. Interictal diffusion and perfusion magnetic resonance imaging features of cats with familial spontaneous epilepsy. *Am J Vet Res* 2017;78:305-310.

3. Sutherland-Smith J, King R, Faissler D, et al. Magnetic resonance imaging apparent diffusion coefficients for histologically confirmed intracranial lesions in dogs. *Vet Radiol Ultrasound* 2011;52:142-148.

4. Hartmann A, Soffler C, Failing K, et al. Diffusion-weighted magnetic resonance imaging of the normal canine brain. *Vet Radiol Ultrasound* 2014;55:592-598.

5. Poyraz AK, Onur MR, Kocakoc E, et al. Diffusion-weighted MRI of fatty liver. *J Magn Reson Imaging* 2012;35:1108-1111.

6. Taouli B, Chouli M, Martin AJ, et al. Chronic hepatitis: role of diffusion-weighted imaging and diffusion tensor imaging for the diagnosis of liver fibrosis and inflammation. *J Magn Reson Imaging* 2008;28:89-95.

7. Manning P, Murphy P, Wang K, et al. Liver histology and diffusion-weighted MRI in children with nonalcoholic fatty liver disease: A MAGNET study. *J Magn Reson Imaging* 2017;46:1149-1158.

8. Anderson SW, Soto JA, Milch HN, et al. Effect of disease progression on liver apparent diffusion coefficient values in a murine model of NASH at 11.7 Tesla MRI. *J Magn Reson Imaging* 2011;33:882-888.

9. Hansmann J, Hernando D, Reeder SB. Fat confounds the observed apparent diffusion coefficient in patients with hepatic steatosis. *Magn Reson Med* 2013;69:545-552.

10. Murphy P, Hooker J, Ang B, et al. Associations between histologic features of nonalcoholic fatty liver disease (NAFLD) and quantitative diffusion-weighted MRI measurements in adults. *J Magn Reson Imaging* 2015;41:1629-1638.

11. Clark MH, Larsen R, Lu W, et al. Investigation of 1H MRS for quantification of hepatic triglyceride in lean and obese cats. *Res Vet Sci* 2013;95:678-680.

12. Johnson KH, Hayden DW, O'Brien TD, et al. Spontaneous diabetes mellitus-islet amyloid complex in adult cats. *Am J Pathol* 1986;125:416-419.

13. Armstrong PJ, Blanchard G. Hepatic lipidosis in cats. *Vet Clin North Am Small Anim Pract* 2009;39:599-616.

14. German AJ. The growing problem of obesity in dogs and cats. *J Nutr* 2006;136:1940S-1946S.

15. Hall JA, Barstad LA, Connor WE. Lipid composition of hepatic and adipose tissues from normal cats and from cats with idiopathic hepatic lipidosis. *J Vet Intern Med* 1997;11:238-242.

16. Ibrahim WH, Bailey N, Sunvold GD, et al. Effects of carnitine and taurine on fatty acid metabolism and lipid accumulation in the liver of cats during weight gain and weight loss. *Am J Vet Res* 2003;64:1265-1277.

17. Springer F, Machann J, Claussen CD, et al. Liver fat content determined by magnetic resonance imaging and spectroscopy. *World J Gastroenterol* 2010;16:1560-1566.

18. Reeder SB, Sirlin CB. Quantification of liver fat with magnetic resonance imaging. *Magn Reson Imaging Clin N Am* 2010;18:337-357, ix.

19. Kuhn JP, Evert M, Friedrich N, et al. Noninvasive quantification of hepatic fat content using three-echo dixon magnetic resonance imaging with correction for T2* relaxation effects. *Invest Radiol* 2011;46:783-789.

20. Bannas P, Kramer H, Hernando D, et al. Quantitative magnetic resonance imaging of hepatic steatosis: Validation in ex vivo human livers. *Hepatology* 2015;62:1444-1455.

21. Peng XG, Ju S, Qin Y, et al. Quantification of liver fat in mice: comparing dual-echo Dixon imaging, chemical shift imaging, and 1H-MR spectroscopy. *J Lipid Res* 2011;52:1847-1855.

22. Hatta T, Fujinaga Y, Kadoya M, et al. Accurate and simple method for quantification of hepatic fat content using magnetic resonance imaging: a prospective study in biopsy-proven nonalcoholic fatty liver disease. *J Gastroenterol* 2010;45:1263-1271.

23. Reeder SB, Cruite I, Hamilton G, et al. Quantitative Assessment of Liver Fat with Magnetic Resonance Imaging and Spectroscopy. *J Magn Reson Imaging* 2011;34:729-749.

24. Del Chicca F, Schwarz A, Meier D, et al. Non-invasive quantification of hepatic fat content in healthy dogs by using proton magnetic resonance spectroscopy and dual gradient echo magnetic resonance imaging. *J Vet Sci* 2018;19:570-576.

25. Lee SS, Park SH, Kim HJ, et al. Non-invasive assessment of hepatic steatosis: prospective comparison of the accuracy of imaging examinations. *J Hepatol* 2010;52:579-585.

26. Bohte AE, van Werven JR, Bipat S, et al. The diagnostic accuracy of US, CT, MRI and 1H-MRS for the evaluation of hepatic steatosis compared with liver biopsy: a meta-analysis. *Eur Radiol* 2011;21:87-97.

27. Serai SD, Dillman JR, Trout AT. Proton Density Fat Fraction Measurements at 1.5- and 3-T Hepatic MR Imaging: Same-Day Agreement among Readers and across Two Imager Manufacturers. *Radiology* 2017;284:244-254.

28. Del Chicca F, Salesov E, Joerger F, et al. Perfusion-weighted and diffusion-weighted magnetic resonance imaging of the liver, spleen, and kidneys of healthy adult male cats. *Am J Vet Res* 2019;80:159-167.

29. Parikh T, Drew SJ, Lee VS, et al. Focal liver lesion detection and characterization with diffusion-weighted MR imaging: comparison with standard breath-hold T2-weighted imaging. *Radiology* 2008;246:812-822.

30. Filipe JP, Curvo-Semedo L, Casalta-Lopes J, et al. Diffusion-weighted imaging of the liver: usefulness of ADC values in the differential diagnosis of focal lesions and effect of ROI methods on ADC measurements. *MAGMA* 2013;26:303-312.

31. Cui Y, Zhang XP, Sun YS, et al. Apparent diffusion coefficient: potential imaging biomarker for prediction and early detection of response to chemotherapy in hepatic metastases. *Radiology* 2008;248:894-900.

32. Koh DM, Scurr E, Collins D, et al. Predicting response of colorectal hepatic metastasis: value of pretreatment apparent diffusion coefficients. *AJR Am J Roentgenol* 2007;188:1001-1008.

33. Taouli B, Beer AJ, Chenevert T, et al. Diffusion-weighted imaging outside the brain: Consensus statement from an ISMRM-sponsored workshop. *J Magn Reson Imaging* 2016;44:521-540.

34. Taouli B, Koh DM. Diffusion-weighted MR imaging of the liver. *Radiology* 2010;254:47-66.

35. Schmeel FC. Variability in quantitative diffusion-weighted MR imaging (DWI) across different scanners and imaging sites: is there a potential consensus that can help reducing the limits of expected bias? *Eur Radiol* 2019;29:2243-2245.

36. Sasaki M, Yamada K, Watanabe Y, et al. Variability in absolute apparent diffusion coefficient values across different platforms may be substantial: a multivendor, multi-institutional comparison study. *Radiology* 2008;249:624-630.

37. Dale BM, Braithwaite AC, Boll DT, et al. Field strength and diffusion encoding technique affect the apparent diffusion coefficient measurements in diffusion-weighted imaging of the abdomen. *Invest Radiol* 2010;45:104-108.

38. Chen ZG, Xu L, Zhang SW, et al. Lesion discrimination with breath-hold hepatic diffusion-weighted imaging: a meta-analysis. *World J Gastroenterol* 2015;21:1621-1627.

39. Saito K, Tajima Y, Harada TL. Diffusion-weighted imaging of the liver: Current applications. *World J Radiol* 2016;8:857-867.

40. Bharwani N, Koh DM. Diffusion-weighted imaging of the liver: an update. *Cancer Imaging* 2013;13:171-185.

41. Chen X, Qin L, Pan D, et al. Liver diffusion-weighted MR imaging: reproducibility comparison of ADC measurements obtained with multiple breath-hold, free-breathing, respiratory-triggered, and navigator-triggered techniques. *Radiology* 2014;271:113-125.

42. Bravo AA, Sheth SG, Chopra S. Liver biopsy. *N Engl J Med* 2001;344:495-500.

43. Kim KY, Song JS, Kannengiesser S, et al. Hepatic fat quantification using the proton density fat fraction (PDFF): utility of free-drawn-PDFF with a large coverage area. *Radiol Med* 2015;120:1083-1093.

44. Ratziu V, Charlotte F, Heurtier A, et al. Sampling variability of liver biopsy in nonalcoholic fatty liver disease. *Gastroenterology* 2005;128:1898-1906.

45. Kleiner DE, Brunt EM, Van Natta M, et al. Design and validation of a histological scoring system for nonalcoholic fatty liver disease. *Hepatology* 2005;41:1313-1321.

46. Rockey DC, Caldwell SH, Goodman ZD, et al. Liver biopsy. *Hepatology* 2009;49:1017-1044.

47. Dillman JR, Trout AT, Costello EN, et al. Quantitative Liver MRI-Biopsy Correlation in Pediatric and Young Adult Patients With Nonalcoholic Fatty Liver Disease: Can One Be Used to Predict the Other? *AJR Am J Roentgenol* 2018;210:166-174.

48. Kise Y, Chikui T, Yamashita Y, et al. Clinical usefulness of the mDIXON Quant the method for estimation of the salivary gland fat fraction: comparison with MR spectroscopy. *Br J Radiol* 2017;90:20160704.

49. Bhat V, Velandai S, Belliappa V, et al. Quantification of Liver Fat with mDIXON Magnetic Resonance Imaging, Comparison with the Computed Tomography and the Biopsy. *J Clin Diagn Res* 2017;11:TC06-TC10.

50. Kukuk GM, Hittatiya K, Sprinkart AM, et al. Comparison between modified Dixon MRI techniques, MR spectroscopic relaxometry, and different histologic quantification methods in the assessment of hepatic steatosis. *Eur Radiol* 2015;25:2869-2879.

51. Kang BK, Kim M, Song SY, et al. Feasibility of modified Dixon MRI techniques for hepatic fat quantification in hepatic disorders: validation with MRS and histology. *Br J Radiol* 2018;91:20170378.

52. Xu L, Duanmu Y, Blake GM, et al. Validation of goose liver fat measurement by QCT and CSE-MRI with biochemical extraction and pathology as reference. *Eur Radiol* 2018;28:2003-2012.

53. Hoy AM, McDonald N, Lennen RJ, et al. Non-invasive assessment of liver disease in rats using multiparametric magnetic resonance imaging: a feasibility study. *Biol Open* 2018;7.

54. Hong CW, Wolfson T, Sy EZ, et al. Optimization of region-of-interest sampling strategies for hepatic MRI proton density fat fraction quantification. *J Magn Reson Imaging* 2018;47:988-994.

55. European Association for the Study of the L, European Association for the Study of D, European Association for the Study of O. EASL-EASD-EASO Clinical Practice Guidelines for the management of non-alcoholic fatty liver disease. *Diabetologia* 2016;59:1121-1140.

56. Shin J, Kim MJ, Shin HJ, et al. Quick assessment with controlled attenuation parameter for hepatic steatosis in children based on MRI-PDFF as the gold standard. *BMC Pediatr* 2019;19:112.

Figure Legends

Figure 1. Colored map derived from the multiple echo GRE sequence in transverse view of one cat of the study at T0 (A, 77 months old, 4.1 kg BW) and T1(B, 40 weeks later, 5.6 kg BW). At T0, the liver was predominantly dark violet. At T1, the liver was predominantly bright violet. Increased subcutaneous and visceral fat tissue is visible at T1. Color scala on the right of the image. Dorsal on the top of the images and right side on the left of the images. Scale bar = 1 cm.

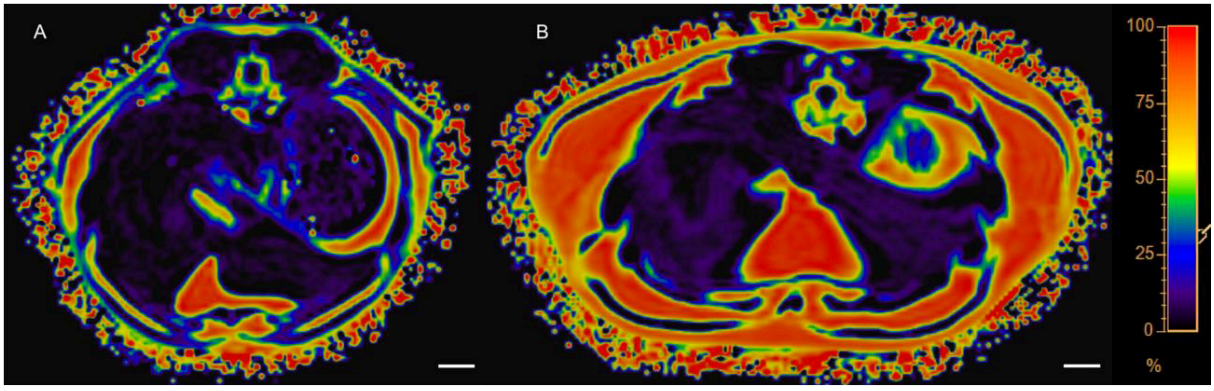

Figure 2. Transverse multiple echo GRE sequence of one cat of the study at T0 (A, 75 months old, 4.6 kg BW) and T1(B, 40 weeks later, 5.8 kg BW). Optically, no difference of the signal intensity of the liver is visible. Estimated HFF in the ROI (white circle in the right

hepatic parenchyma) was 3.3% at T0 and 4.18% at T1. Increased subcutaneous and visceral fat tissue is visible at T1. Dorsal on the top of the image and right side on the left of the image.

Scale bar = 1 cm.

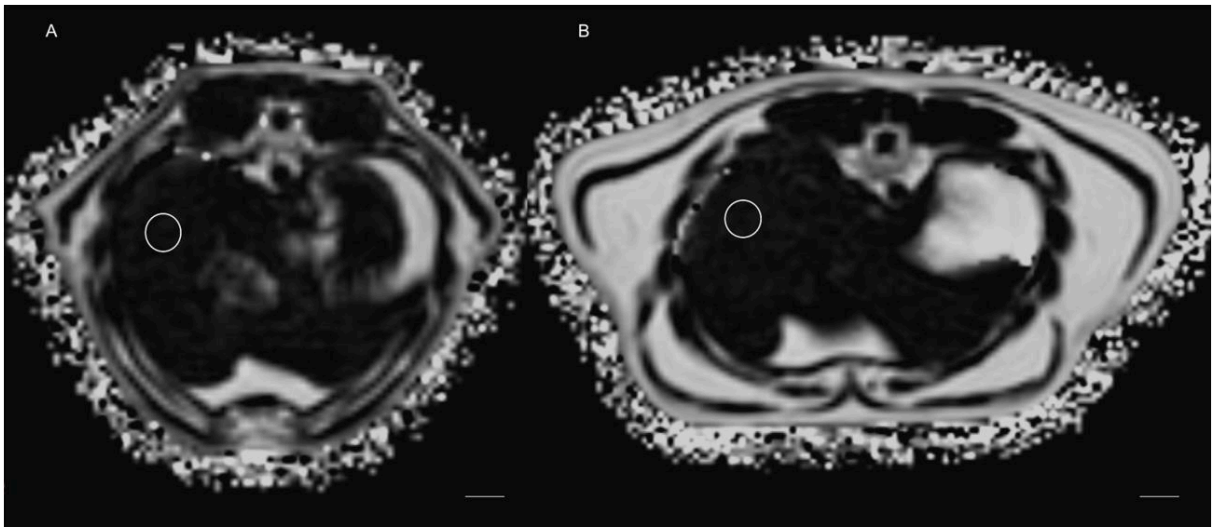

Figure 3. ADC map in transverse view of the liver of one cat of the study at T0 (A, 75 months old, 4.7 kg BW, HFF 3.13%) and T1 (B, 40 weeks later, 6.5 kg BW, HFF 4.12%). Optically, no difference of the signal intensity of the ADC map is visible. Measured ADC on the ROI (white circle in the right liver parenchyma) was 1.19×10^{-3} mm^2/s at T0 and 0.9×10^{-3} mm^2/s at T1. The limited spatial resolution is visible. Dorsal on the top of the image and right side on the left of the image. Scale bar = 1 cm. GB, gallbladder.

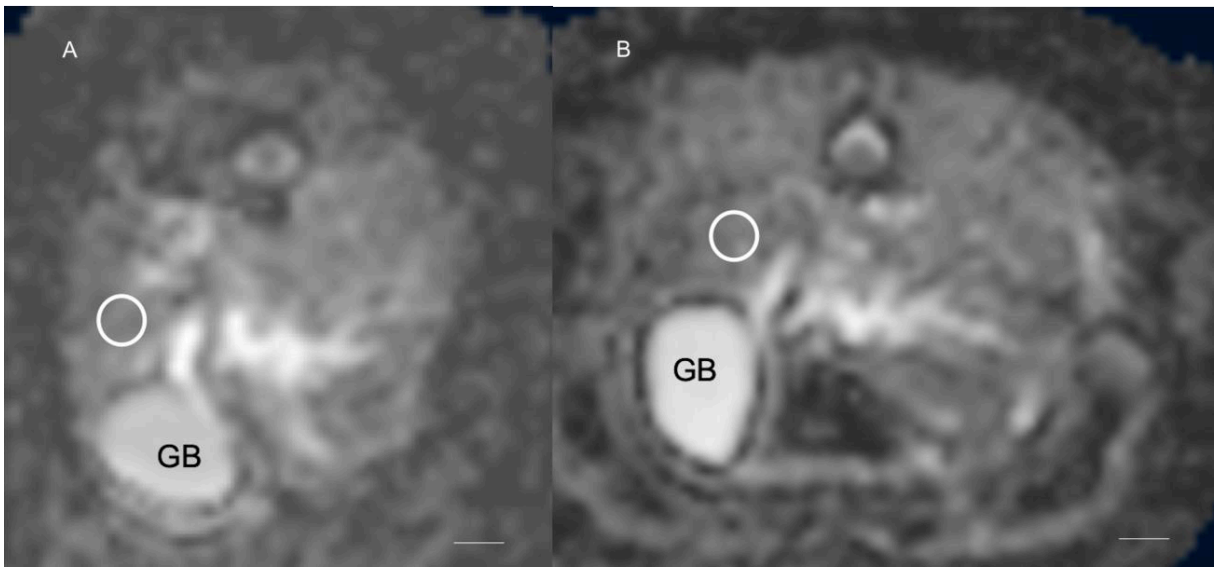

Figure 4: Box plots of the mean BW, HFF, and ADC at T0 and T1. BW_T0 and BW_T1 expressed in kg; HFF_T0 and HFF_T1 expressed in %; ADC_T0 and ADC_T1 expressed in unit × 10^{-3} mm^2/s.

For each plot, the box represents the 25th to 75th percentiles, and the dark line represents the median; the dots represent the single values.

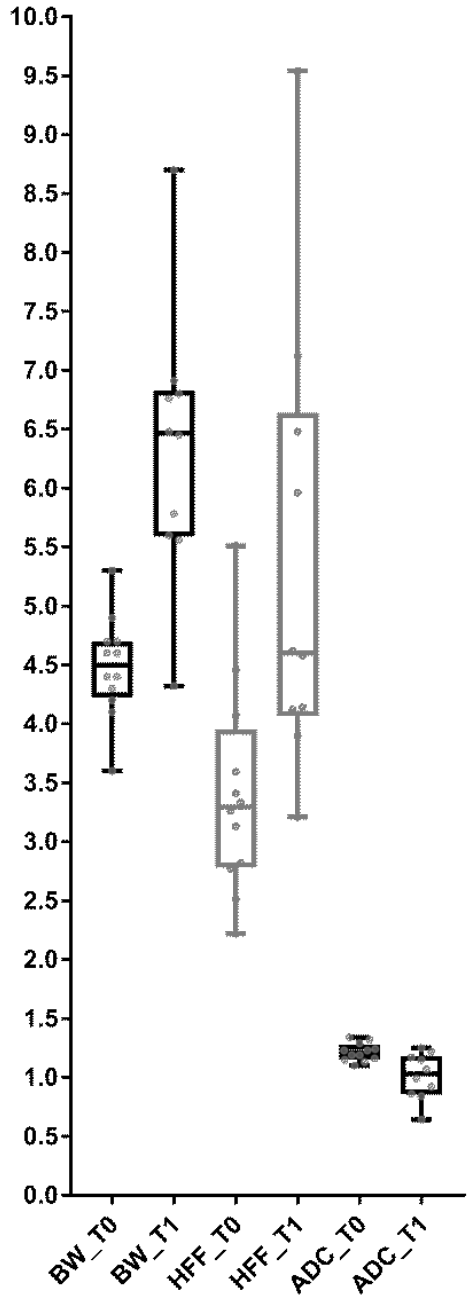

Danksagung

An dieser Stelle möchte ich allen Personen, die mich bei der Anfertigung meiner Dissertation unterstützt haben und insbesondere Francesca del Chicca und Patrick Kircher meinen Dank aussprechen.

Ganz besonderen Dank gebührt auch meinen Grosseltern, Eltern, Schwestern und meiner Partnerin.

Curriculum Vitae

Vorname Name	Gian-Luca Marcus Steger
Geburtsdatum	11.12.1993
Geburtsort	Chur, Schweiz
Nationalität	Schweiz
Heimatort bei Schweizern	Chur
Aug. 2000 – Juni 2006	Primarschule (Schulhaus Masans, Chur, Schweiz)
Aug. 2006 – Juni 2008	Sekundarschule (Schulhaus Quader, Chur, Schweiz)
Aug. 2008 – Juni 2012	Kantonsschule (Bündner Kantonsschule, Chur, Schweiz)
30.06.2012	Matura (Bündner Kantonsschule, Chur, Schweiz)
Aug. 2012 – Juli 2015	Bachelor (Veterinärmedizin, Universität Zürich, Zürich, Schweiz)
Aug. 2015 – Juli 2018	Master (Veterinärmedizin, Universität Zürich, Zürich, Schweiz)
29. Dez. 2017	Abschlussprüfung vet. med. (Universität Zürich, Zürich, Schweiz)
Mai 2018 – Heute	Anfertigung der Dissertation Unter Leitung von Patrick R. Kircher, Prof. Dr. med. vet., PhD, Dipl. ECVDI, exec. MBA (UZH) am Departement für klinische Diagnostik und Services der Vetsuisse-Fakultät Universität Zürich Patrick R. Kircher, Prof. Dr. med. vet., PhD, Dipl. ECVDI, exec. MBA (UZH)
Nov. 2018 – Feb. 2020	Assistenztierarzt in Weiterbildung zum Fachtierarzt FVH für Kleintiere, Tierklinik Masans, Chur, Schweiz